Octupole correlations in the transitional actinides and the *spdf* interacting boson model

N. V. Zamfir[1,2,3] and Dimitri Kusnezov[4]
[1]*Wright Nuclear Structure Laboratory, Yale University, New Haven, Connecticut 06520-8124*
[2]*Clark University, Worcester, Massachusetts 01610*
[3]*National Institute for Physics and Nuclear Engineering, Bucharest-Magurele, Romania*
[4]*Sloane Laboratory, Yale University, New Haven, Connecticut 06520*
(Received 7 December 2000; published 10 April 2001)

The region of light actinides ($Z\sim88$,$N\sim134$), which is thought to exhibit signs of stable octupole deformation, offers a real challenge for nuclear structure models. We study the even-even Ra-Th nuclei in the framework of the *spdf* interacting boson model and we find that while the properties of the low-lying states can be understood without stable octupole deformation, higher spin states ($J\gtrsim12\hbar$) in some of these nuclei (e.g., ^{226}Ra) suggest that octupole deformation develops with increasing spin. We also discuss how octupole deformation can arise in the rotational (dynamical symmetry) limit.

DOI: 10.1103/PhysRevC.63.054306 PACS number(s): 21.60.Fw, 21.10.Re, 23.20.Lv, 27.90.+b

I. INTRODUCTION

Nuclear octupole states, despite nearly 50 years of history, are much less understood than quadrupole collective states. The question of the existence of octupole deformation is challenging for nuclear structure models. The difficulty arises from the fact that there are no specific established phenomenological criteria for the degree of octupole collectivity. Although there are many models [1], microscopic or macroscopic, geometrical or algebraic, there is yet no definite answer as to which nuclei are octupole deformed, if any, or which models adequately describe the occurrence of strong octupole correlations.

Extensive and numerous experimental and theoretical studies were dedicated over the years to the study of the light actinides where it has been argued that the nuclei around $Z\sim88$,$N\sim134$ might present intrinsic octupole deformation [1,2]. In the even-even nuclei in this region, alternating parity bands, $K^\pi=0_1^+$ and $K^\pi=0_1^-$, which are thought to indicate the presence of stable octupole deformation, have been observed. However, the question of the existence of octupole deformation is still very much open and different empirical signatures are controversial. The recent developments in spectroscopic techniques have produced qualitatively new sets of data that constitute a real challenge for different models and extensive numerical studies are necessary to test their ability to describe the experimental features. A suitable and versatile model for the description of quadrupole-octupole collective degrees of freedom is the interacting boson model [3]. The aim of this work is to obtain the simplest systematic description of a large region of transitional even-even nuclei ($Z=86-90$, $N=130-142$) and to test whether octupole deformation is necessary and where it should appear.

II. *spdf* INTERACTING BOSON MODEL CALCULATIONS

The interacting boson model (IBM) offers a phenomenological approach of collective nuclear structure by introducing bosons of a given spin that are associated with the corresponding multipole modes. The quadrupole vibrations and deformations are described in terms of interacting *s* and *d* bosons with $L^\pi=0^+$ and $L^\pi=2^+$, respectively. Negative parity states are described by introducing bosons with odd values of angular momentum. Attempts to describe both the quadrupole and the octupole excitations were already proposed at an early stage in the development of the model [4,5]. The $f(L^\pi=3^-)$ boson has been introduced in addition to the standard *s* and *d* bosons. As long as only octupole vibrations are considered, the introduction of only one *f* boson appears to be sufficient to describe the octupole vibrational bands in quadrupole deformed nuclei [6–8]. However, in order to describe the low-lying $K=0^-$ bands in transitional actinides, $p(L^\pi=1^-)$ bosons were considered. The *spdf* version of the IBM was introduced by Han *et al.* [9] and by Engel and Iachello [10]. Since the entire model space is very large, different truncations of the Hilbert space or/and the Hamiltonian have been applied and a variety of data successfully explained in the rare-earth nuclei [11–14] and in the actinides [15–18]. However, the recent increase in the amount of available data in transitional actinides makes a systematic study of the entire region very interesting and challenging.

From the algebraic point of view, the introduction of the *p* boson along with the *f* boson leads to many new symmetries. Dynamical symmetries of the related group, U(16), were studied by Nadjakov and Mikhailov [20] and completely constructed and classified by Kusnezov [11,19]. By coupling the *f* boson algebra to the *sd* space of U(6), no nontrivial dynamical symmetries are realized. Introducing the additional *p* boson, one obtains new symmetries, including vibrational, rotational, and γ-soft structures in the full *spdf* space [19]. We are interested in studying the behavior of negative parity states in a region where the positive parity states are undergoing a transition from vibrators [$U_{sd}(5)$] to rotors [$SU_{sd}(3)$]. The existence of the $U_{spdf}(5)$ and $SU_{spdf}(3)$ limits in the full space allows us to study this transition treating positive and negative parity states on equal footing.

Although, the introduction of *p* bosons appears to be dictated by the underlying microscopic structure [21], there is no clear understanding of its nature. Engel and Iachello [10] considered that the origin of the *p* boson could be a possible correction of the spurious center-of-mass motion of the

quadrupole-octupole intrinsic system. Otsuka and Sugita [15], on the other hand, have argued that correction for the spurious center-of-mass motion introduced by the p boson is of the order of $O(1/A)$, which is negligible in the first approximation in heavy nuclei. Sugita *et al.* [14] considered that the p boson is related to the giant dipole resonance (GDR), thus the p boson energy ($\sim$15 MeV) is very high compared to the energy of the other bosons ($\leqslant$1.5 MeV). A similar idea was used to show that the coupling of the GDR states (p boson states) to the octupole-vibration states (f boson states) is responsible for the existence of the two-body terms in the sdf $E1$ operator [22], terms that are necessary in order to explain the $E1$ data in quadrupole deformed nuclei in the framework of the sdf IBM. Despite all these studies, the justification and the physical significance of the p boson still remain open questions.

Even though the dynamical symmetries of the sd IBM constituted benchmarks for the phenomenology of the quadrupole collectivity, in the case of octupole collectivity none of the dynamical symmetries of the $spdf$ model have been fully exploited. The $Z\sim 88, N\sim 134$ nuclei provide a good test of the model due to the wealth of experimental information. In addition, it is also a region where octupole deformation has been predicted by microscopic-macroscopic calculations [2] to play a role in the behavior of the collective negative parity states. In this way the low-lying negative parity states in the light actinides could constitute a severe test of the extension of the pf basis necessary to explain the data.

Since these nuclei are undergoing a structural transition, a dynamical symmetry approach is not suitable and numerical calculations are needed. The structure of the positive parity states in the light actinides is changing from the vibrational to the rotational structure (the number of bosons, N_B, increases from 5 to 12). This type of structural change is well explained by a simple Hamiltonian [23,24] $H_{sd}=\epsilon_d\hat{n}_d - \kappa\hat{Q}_{sd}\cdot\hat{Q}_{sd}$. We assume that the same degrees of freedom will describe the evolution of the negative parity states as well. The Hamiltonian that contains the essential degrees of freedom of the evolution from vibrational to rotational structure is

$$H=\epsilon_d\hat{n}_d+\epsilon_p\hat{n}_p+\epsilon_f\hat{n}_f-\kappa\hat{Q}_{spdf}\cdot\hat{Q}_{spdf}, \tag{1}$$

where ϵ_p, ϵ_d, and ϵ_f are the boson energies and $\hat{n}_p=-p^\dagger\cdot\tilde{p}$, $\hat{n}_d=d^\dagger\cdot\tilde{d}$, and $\hat{n}_f=-f^\dagger\cdot\tilde{f}$ are the boson number operators. The quadrupole operator

$$\begin{aligned}\hat{Q}_{spdf}&=\hat{Q}_{sd}+\hat{Q}_{pf}\\&=[s^\dagger\tilde{d}+d^\dagger s]+\chi_{sd}^{(2)}[d^\dagger\tilde{d}]^{(2)}+\frac{3\sqrt{7}}{5}[p^\dagger\tilde{f}+f^\dagger\tilde{p}]^{(2)}\\&\quad+\chi_{pf}^{(2)}\left\{\frac{9\sqrt{3}}{10}[p^\dagger\tilde{p}]^{(2)}+\frac{3\sqrt{42}}{10}[f^\dagger\tilde{f}]^{(2)}\right\}\end{aligned} \tag{2}$$

with $\chi_{sd}^{(2)}=\pm\sqrt{7}/2$ and $\chi_{pf}^{(2)}=\pm 1$ is related to the Casimir operator of the $SU_{spdf}(3)$ subgroup of $U_{spdf}(16)$. We note that the equally good choice $\hat{Q}_{spdf}=\hat{Q}_{sd}-\hat{Q}_{pf}$ leads to identical results, the energy levels being invariant with respect to this relative sign between the quadrupole operators. Concerning the sign of $\chi_{pf}^{(2)}$, we obtained a better fit with $\chi_{pf}^{(2)}=-1$ (for $\chi_{sd}^{(2)}=-\sqrt{7}/2$) [i.e., $\mathrm{sgn}(\chi_{sd}^{(2)},\chi_{pf}^{(2)})=(-,-)$]. Identical results for spectra and electromagnetic transitions are obtained with $\mathrm{sgn}(\chi_{sd}^{(2)},\chi_{pf}^{(2)})=(+,+)$. Completely different results (see the discussion later related to the rotational dynamical symmetry limit in Sec. III) would be obtained if $\mathrm{sgn}(\chi_{sd}^{(2)},\chi_{pf}^{(2)})=(+,-)$ or $(-,+)$.

This Hamiltonian has a well-defined vibrational limit, characterized by the vibrational operators $\hat{n}_p$, $\hat{n}_d$, and $\hat{n}_f$, and the algebraic structure of the vibrational limit is simply

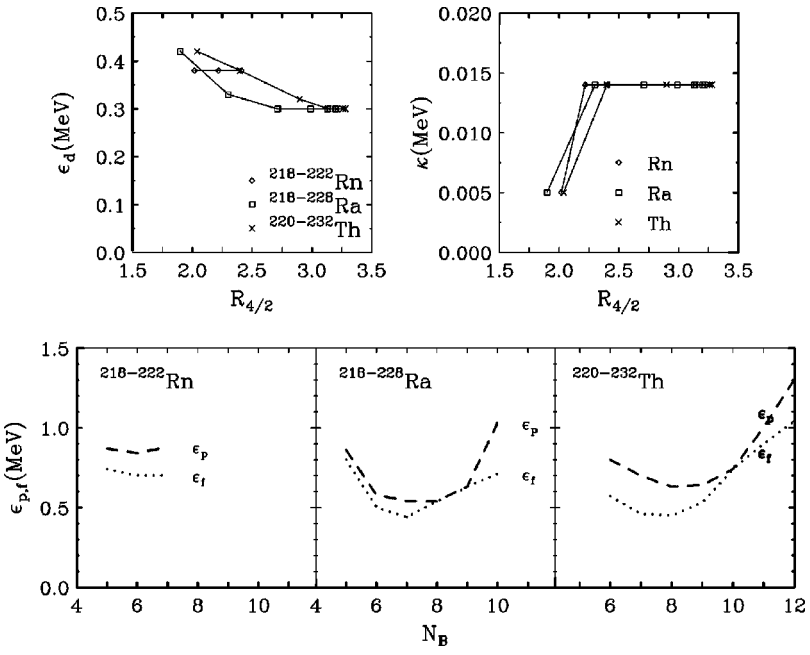

FIG. 1. The parameters of the $spdf$ Hamiltonian of Eq. (1) used for Rn, Ra, and Th isotopic chains. Top: The d-boson energy (ϵ_d) and the strength of the quadrupole-quadrupole term (κ) as a function of $R_{4/2}\equiv E(4_1^+)/E(2_1^+)$ showing that for spherical nuclei ($R_{4/2}\sim 2.0$) ϵ_d is large ($\sim$0.4 MeV) and κ is small (0.005 MeV) and for transitional and quadrupole deformed nuclei ($R_{4/2}>2.5$) ϵ_d is lower ($\sim$0.3 MeV) and κ is larger (0.014 MeV). Bottom: The energy of the p and f bosons ($\epsilon_{p,f}$) as a function of boson number N_B.

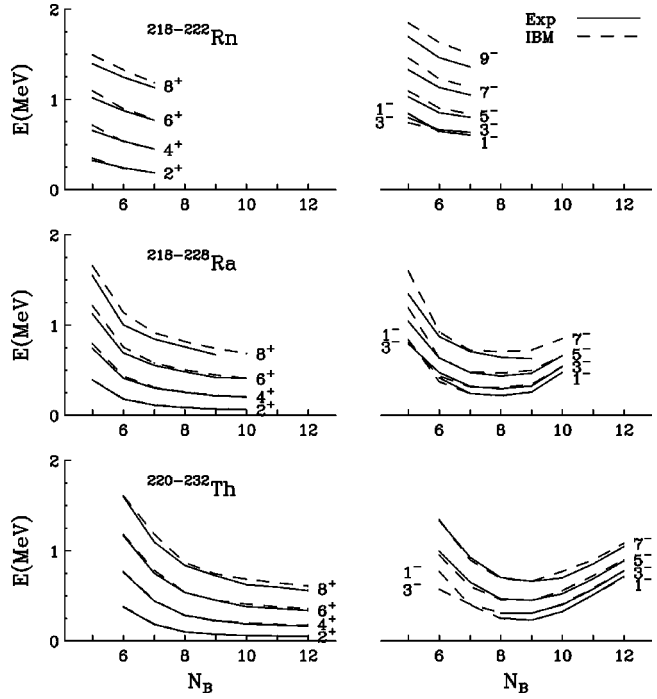

FIG. 2. Experimental [27–43] (continuous lines) and calculated (dashed lines) energies for the $K^\pi = 0_1^+, 0_1^-$ bands.

the product of the independent harmonic oscillator algebras for each type of boson. The rotational structure is generated by $\hat{Q}^2_{spdf}$. The same strength κ of the quadrupole interaction describes the sd bosons and the pf bosons as well. This form of the quadrupole operator treats all bosons equally. The cross term of $\hat{Q}^2_{spdf}$, given by $2\hat{Q}_{sd}\cdot\hat{Q}_{pf}$, provides a quadrupole-quadrupole interaction between the positive and negative parity bosons. All the terms in our Hamiltonian [Eq. (1)] are diagonal in the $U_{spdf}(16) \supset U_{sd}(6) \otimes U_{pf}(10)$ basis and consequently the numbers of positive (N_+) and negative parity (N_-) bosons are separately conserved.

A. Dipole-octupole vibrations

The calculations were done with the code OCTUPOLE [25]. We start the study with only one pf boson. For the parameter choices below, we will see that this is a good approximation of the full space calculations for the low-energy states. The Hamiltonian parameters (three boson energies ϵ_d, ϵ_p, and ϵ_f and the strength κ of the quadrupole-quadrupole interaction) are shown in Fig. 1. They have a smooth behavior across the region: ϵ_d varies from 0.38–0.42 MeV for vibrational nuclei [$R_{4/2} \equiv E(4_1^+)/E(2_1^+) \sim 2.0$] to 0.30 MeV for rotational nuclei ($R_{4/2} \sim 3.33$). The parameters ϵ_p and ϵ_f vary between 0.5 and 1.3 MeV and they behave very similar, with ϵ_p slightly higher, with a minimum for $N_B \sim 8$. It is worth noting that near this minimum $\epsilon_p = \epsilon_f$ and these nuclei (^{224,226}Ra and ^{228}Th) are precisely those where octupole deformation is suspected to be strongest. $\epsilon_p = \epsilon_f$ has particular significance for our Hamiltonian and we will return to this issue in Sec. III. The strength κ of the quadrupole-quadrupole interaction has the same value (0.014 MeV) for almost all nuclei considered in this fit except the most spherical ones where, as one expects, the value is much smaller (0.005 MeV). This ϵ_d, κ behavior is consistent with the behavior seen in transitional nuclei [26].

In Fig. 2 we present a comparison of the calculated (dashed) and experimental (solid) spectra. Here and in the following figures the data are from Refs. [27–43]. The alternating parity yrast bands ($K^\pi = 0_1^+$ and $K^\pi = 0_1^-$) for these transitional nuclei are very nicely reproduced. The agreement is also very good for vibrational nuclei ($N_B = 5,6$) including the inversion of the 1^- and 3^- states (the 3^- state is lower than 1^- in ^{218}Rn [27] and ^{218}Ra [28] and is higher in all other nuclei).

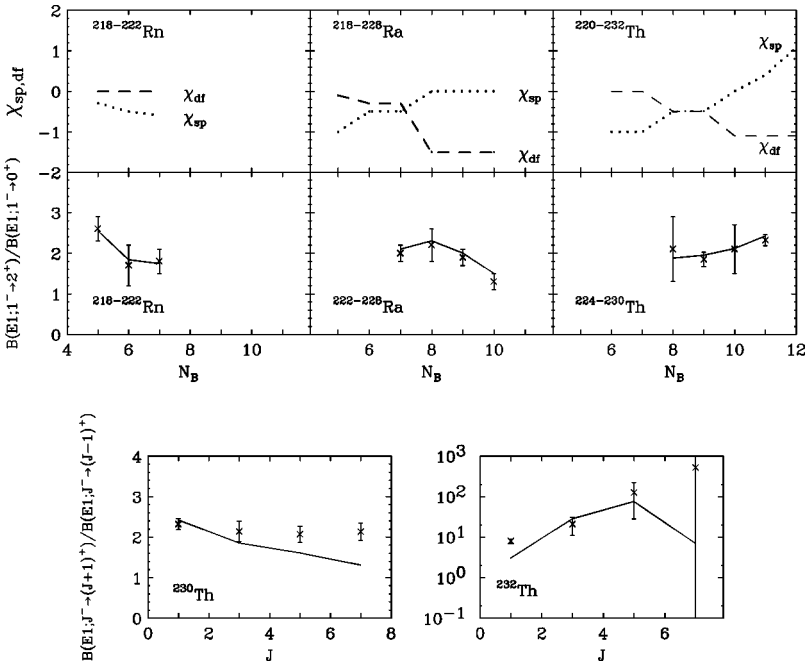

FIG. 3. Top: The parameters $\chi^{(1)}_{sp}$ and $\chi^{(1)}_{df}$ of the $T(E1)$ operator of Eq. (3) used to calculate the transition rates in the Rn, Ra, and Th isotopic chains. Middle: Experimental (symbols) and theoretical (continuous lines) $B(E1)$ branching ratio from 1_1^- states. Bottom: Similar to the middle panels but for $B(E1)$ branching ratios from $J \geqslant 1^-$ states in ^{230,232}Th.

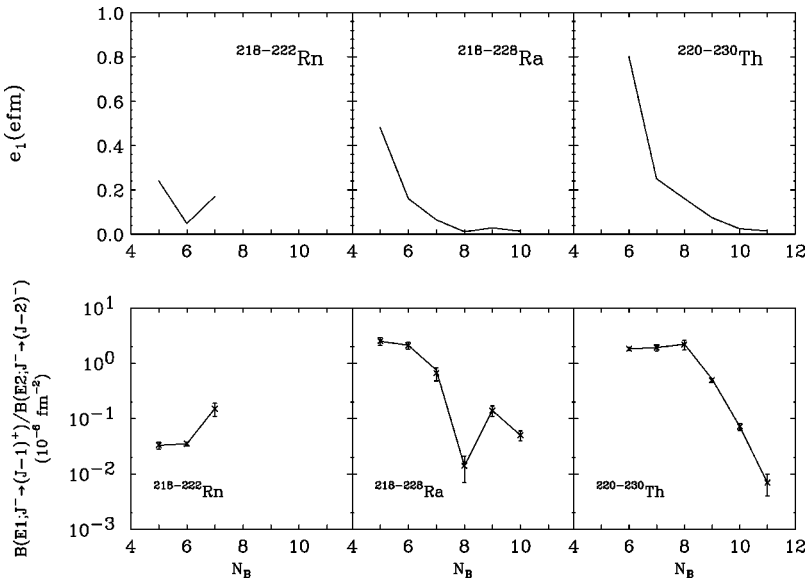

FIG. 4. Top: The effective charge e_1 used to calculate the $E1$ transition rates. The other $E1$ parameters, $\chi_{sp}^{(1)}$ and $\chi_{df}^{(1)}$ are presented in Fig. 3 (top). Bottom: Experimental (symbols) and theoretical (continuous lines) spin averaged values for the $B(E1)/B(E2)$ ratio. A single value for e_2 was used, obtained from the fit of the known $B(E2)$ experimental values in these isotopes, $e_2 = 0.18\,e$ b, but only a mass dependent e_1, presented in the top part of the figure, reproduces the experimental points.

$E1$ transitions are studied using the one-body operator

$$T_{spdf}^{(E1)} = e_1([p^\dagger \tilde{d} + d^\dagger \tilde{p}]^{(1)} + \chi_{sp}^{(1)}[s^\dagger \tilde{p} + p^\dagger s]^{(1)} + \chi_{df}^{(1)}[d^\dagger \tilde{f} + f^\dagger \tilde{d}]^{(1)}). \quad (3)$$

The $E1$ branching ratios depend only on $\chi_{sp}^{(1)}, \chi_{df}^{(1)}$ and are not dependent on the effective charge e_1. The parameters $\chi_{sp}^{(1)}, \chi_{df}^{(1)}$ that fit the data are presented in Fig. 3 (top). Their values across the three isotopic chains show a smooth evolution. They indicate also that the balance between the three terms in the $E1$ operator in Eq. (3) is different for vibrational, transitional or rotational nuclei.

In Fig. 3 (middle) we compare the data and the IBM calculations for the branching ratio $B(E1;1_1^- \rightarrow 2_1^+)/B(E1;1_1^- \rightarrow 0_1^+)$ for different isotopic chains and in Fig. 3 (bottom) for the branching ratios $B(E1;J^- \rightarrow [J+1]^+)/B(E1;J^- \rightarrow [J-1]^+)$ as a function of spin for ^{230,232}Th. In all cases the agreement with the data is excellent, including the large variation in magnitude of the branching ratio as a function of spin in ^{232}Th.

Another test of the model constitutes the $B(E1)/B(E2)$ ratios. For the $T(E2)$ operator we used the full $spdf$ form, namely, $T(E2) = e_2 \hat{Q}_{spdf}$. The effective charge $e_2 = 0.18\,e$ b is the same for all nuclei and is obtained from the fit of all known $B(E2)$ experimental values. The evolution in spin of the experimental $B(E1)/B(E2)$ ratios in these nuclei is fairly constant (within errors). Consequently, in Fig. 4 (bottom) we compare the experimental and theoretical spin averaged $B(E1)/B(E2)$ ratios. The agreement is obtained with a mass dependent effective charge e_1 presented in Fig. 4 (top). We note that the smaller value of the $B(E1)/B(E2)$ ratio for ^{224}Ra compared with that in the neighboring isotopes is reproduced only by considering a slightly smaller effective charge.

The wealth of data in ^{226}Ra [37] offers the possibility of an extensive comparison of the $E1$ and $E3$ matrix elements. In Fig. 5 the experimental $E1$ matrix elements are compared with our calculations. The results with $1pf$ are represented by the dashed line. The $E1$ parameters are the same as those used in calculating the branching ratios for ^{226}Ra in Figs. 3 and 4, namely, $\chi_{sp}^{(1)} = 0, \chi_{df}^{(1)} = -1.5$, and $e_1 = 0.023\,e$ fm. The agreement is reasonable except the staggering behavior of the calculated matrix elements at high spins. This effect could be a consequence of an incomplete p-f content in these states and, as we will see later, this could be corrected by a small additional interaction, which requires the extension of the model space to more pf bosons.

In Fig. 6 we show the comparison between the experimental $E3$ matrix elements in ^{226}Ra with the calculations. The $E3$ operator is

$$T_{spdf}^{(E3)} = e_3([d^\dagger \tilde{f} + f^\dagger \tilde{d}]^{(3)} + \chi_{pd}^{(3)}[p^\dagger \tilde{d} + d^\dagger \tilde{p}]^{(3)} + \chi_{sf}^{(3)}[s^\dagger \tilde{f} + f^\dagger s]^{(3)}). \quad (4)$$

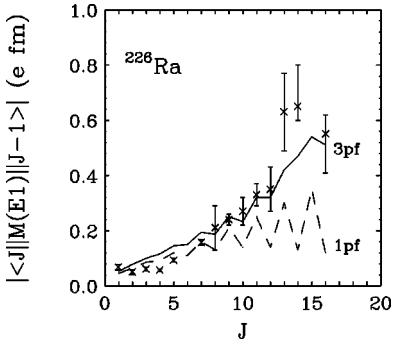

FIG. 5. Comparison of the experimental $E1$ matrix elements [37] (symbols) with IBM calculations with $1pf$ boson (dashed line) and $3pf$ bosons (continuous line). The Hamiltonian for the $3pf$ boson calculation was obtained by adding a very small dipole-dipole interaction ($\alpha = 0.0005$ MeV) [Eq. (5)] to the Hamiltonian in Eq. (1). The parameters for the $E1$ transition operator are the same as those used to calculate the branching ratios for ^{226}Ra in Figs. 3 and 4.

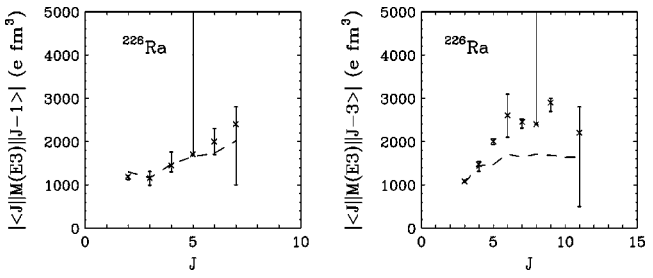

FIG. 6. Comparison of the experimental $E3$ matrix elements [37] (symbols) with 1-pf IBM calculations (dashed line). The parameters of the $E3$ operator in Eq. (4) are $e_3=22.6\,e$ fm^3, $\chi_{pd}^{(3)}=-1$, $\chi_{sf}^{(3)}=0$.

Since the data on $E3$ matrix elements are limited to ^{226}Ra it is not possible to search for a smoothly varying set of $E3$ parameters across the region. We present in Fig. 6 the theoretical $E3$ matrix elements obtained with $e_3=22.6\,e$ fm^3, $\chi_{pd}^{(3)}=-1$, and $\chi_{sf}^{(3)}=0$.

The comparisons presented in Figs. 2–6 show that calculations with $1pf$ boson are able to reproduce the essential features of the alternating parity bands in the light actinides at least at low spin.

In order to see if the p boson is essential or not in describing the negative parity states we show in Fig. 7 a comparison of two sets of calculations corresponding to ^{230}Th: One calculation uses the $1pf$ boson approach described in the present work and the other is a $1f$ description from Ref. [8]. Although the general pattern is similar, the $spdf$ calculation better describes the position of the $K^\pi=0_2^+$ band, i.e., lower than $K^\pi=2_\gamma^+$. This could be partially due to slightly different parameters giving rise to the positive parity states. The effect on the calculated $B(E1)$ branching ratios is presented in Table I, where a full comparison of the two calculations is made with all the experimentally known $B(E1)$ branching ratios in ^{230}Th. The two calculations agree with the experimental values except those when one of the transitions is to the $K^\pi=0_2^+$ band when both sets fail to reproduce the data.

In comparison with only one f boson, the addition of one p boson does not change the essential features of the agreement with the data at least for deformed nuclei as ^{230}Th. Extending the basis to $3pf$ bosons does not improve the agreement either. In lighter nuclei, ^{222,224}Ra and ^{226,228}Th, where the $K^\pi=0_2^+$ bandhead is known, the $1pf$ calculations with the parameters in Fig. 1 predict too low (by 100–200 keV) 0_2^+ states. However, a slight change in the parameters (without keeping the same κ and $\chi_{sd}^{(2)}$ values for all nonspherical nuclei) would improve the agreement. More data on $K^\pi=0^+$ and other nonyrast states in these nuclei are necessary in order to obtain unambiguous parameters and to make possible an extensive comparison of different calculations with $1f$ or $1pf$ bosons.

B. Dipole-octupole deformation

The calculations presented so far do not imply a dipole-octupole deformation, i.e., with only $1pf$ boson in the calculations there are no negative parity bosons in the positive parity states. The ground state may only have a quadrupole deformation and the negative parity states are built by dipole-octupole vibrations on top of this ground state. In order to see the effect of the presence of pf bosons in the positive parity yrast states, we extend the basis by allowing three negative parity bosons. However, the Hamiltonian of Eq. (1) conserves separately the number of sd and pf bosons. Thus the positive parity states composed of $(pf)^2$ components will not interact with positive parity states with no pf bosons, such as the ground state band. This can be achieved by introducing a simple interaction which in contrast to the $\hat{Q}_{sd}\cdot\hat{Q}_{sd}$ interaction, is not diagonal in the $U_{spdf}(16)\supset U_{sd}(6)\otimes U_{pf}(10)$ basis and, hence, mixes the positive parity states with different pf components. This type of mixing could be achieved by a dipole-dipole interaction of the form

$$H_{int}=\alpha\hat{D}_{spdf}^{\dagger}\cdot\hat{D}_{spdf}+\text{H.c.}, \tag{5}$$

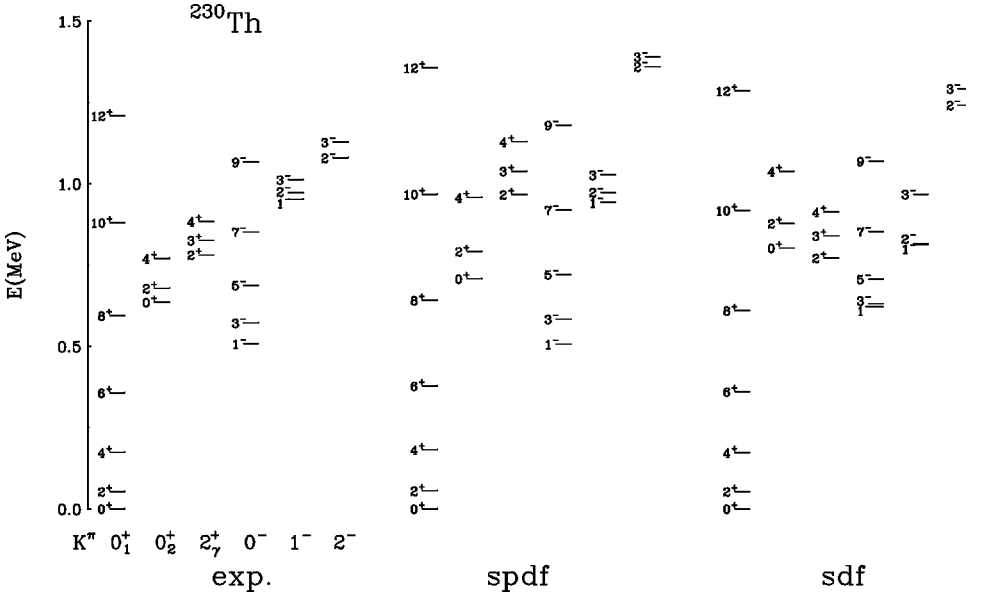

FIG. 7. Experimental values for the energies of different bands in ^{230}Th compared with $spdf$ (present work) and sdf [8] calculations.

TABLE I. $B(E1;J_i^- \rightarrow J_{f1}^+)/B(E1;J_i^- \rightarrow J_{f2}^+)$ for octupole bands in ^{230}Th compared with calculations in the $1pf$ and $1f$ limits of the IBM.

K^-	J_i^-	J_{f1}^+	J_{f2}^+	Exp	$1pf$	$1f$ [8]
0^-	1^-	2_1^+	0_1^+	2.32(14)	2.42	2.60
	3^-	4_1^+	2_1^+	2.15(24)	1.85	1.65
	5^-	6_1^+	4_1^+	2.06(19)	1.61	1.21
	7^-	8_1^+	6_1^+	2.12(24)	1.31	0.92
1^-	1^-	2_1^+	0_{gs}^+	0.24(2)	0.44	0.17
	1^-	$2_{K=0_2^+}^+$	2_1^+	0.6(2)	114	2.7
	3^-	4_1^+	2_1^+	0.09(4)	0.04	0.54
2^-	2^-	$2_{K=0_2^+}^+$	2_1^+	0.28(7)	0.12	1.64
	2^-	2_γ^+	2_1^+	1.2(6)	3.8	0.9
	2^-	3_γ^+	2_γ^+	0.8(5)	0.3	0.8
	3^-	4_1^+	2_1^+	0.31(9)	0.07	0.89
	3^-	$2_{K=0_2^+}^+$	2_1^+	$\simeq 0.2$	48	0.05
	3^-	2_γ^+	2_1^+	<1.1	0.01	1.8

where

$$\hat{D}^{(1)}_{spdf} = -2\sqrt{2}[p^\dagger \tilde{d} + d^\dagger \tilde{p}]^{(1)} + \sqrt{5}[s^\dagger \tilde{p} + p^\dagger s]^{(1)} + \sqrt{7}[d^\dagger \tilde{f} + f^\dagger \tilde{d}]^{(1)}) \quad (6)$$

is the dipole operator arising from the $O(4)$ dynamical symmetry limit, which does not conserve separately the number of positive and negative parity bosons [19].

The calculations with the new Hamiltonian obtained by adding H_{int} to the Hamiltonian in Eq. (1) and with an extended basis (up to $3pf$ bosons) change only slightly the previous results. In Fig. 8 we compare the experimental energy spectrum of ^{226}Ra with the IBM calculations with $1pf$ and $3pf$ bosons. In the case of three negative parity bosons we added an interaction term (5) with a very small strength, $\alpha = 0.0005$ MeV, to the Hamiltonian of Eq. (1). The two sets of calculations produce very similar yrast energies. The $B(E1)$ branching ratios are reproduced with the same set of parameters values. However, the absolute $E1$ matrix elements are slightly changed and the variation with spin is much better reproduced (the continuous line in Fig. 5). Thus, the yrast structure changes modestly with an improvement of the detailed behavior of the $E1$ transition rates at high spin. However, the nonyrast structure is changed dramatically; The density of nonyrast states is higher and an additional positive parity band, labeled ''3'' in Fig. 8, containing $2pf$ bosons is predicted at ~ 0.5 MeV. This band is primarly composed of $(pf)^2$ bosons at low spin. However in the fig-

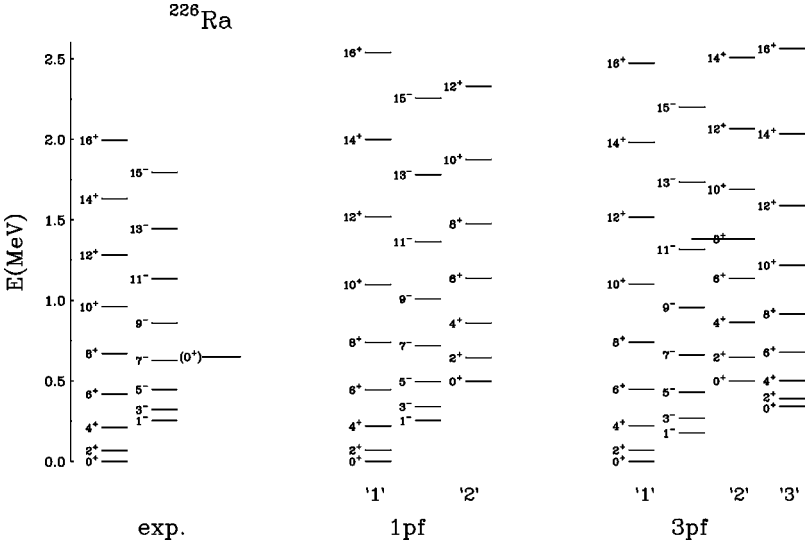

FIG. 8. Comparison of the experimental spectrum of ^{226}Ra with $1pf$ and $3pf$ calculations. The first two $K^\pi = 0^+$ bands in the $1pf$ calculation are labeled ''1'' and ''2.'' In the $3pf$ calculation an additional $K^\pi = 0^+$ band of $(pf)^2$ character at low spin appears near 0.5 MeV and is labeled ''3.'' The levels within a band are connected via strong $B(E2)$ values and, as a consequence, the (pf) content of bands ''1'' and ''3'' interchange near $J^\pi \sim 12\hbar$ (see Fig. 9).

ure, the bands are organized according to the $B(E2)$ strength. Near $J\sim 12\hbar$, the states in bands ''1'' and ''3'' mix strongly and above 12^+, the $(pf)^2$ character of the wave functions becomes yrast and now appears in band ''1.'' Hence, the dipole-dipole interactions induces p,f components in the wave functions of the yrast states. Figure 9 shows that the amount of negative parity bosons in yrast states, i.e., the dipole-octupole deformation is increasing with spin with a sudden increase at spin $J\sim 12\hbar$. The lack of experimental data on nonyrast states prevent us to draw any definite conclusion about the exact contribution of the full space relative to only $1pf$ boson. In rotational nuclei, like ^{230}Th, where nonyrast states are known, extending the basis to $3pf$ bosons does not improve the agreement. It seems that more interactions must be added to the Hamiltonian (1) in order to describe the nonyrast states in these nuclei.

III. ROTATIONAL DYNAMICAL SYMMETRY

As was mentioned above, the introduction of the p boson along with the f boson leads to many new symmetries [19]. Although the Hamiltonian in Eq. (1) describes the transition from vibrator to rotor, the presence of all terms in the calculations prevents in general the appearance of a dynamical symmetry. There is a notable exception: in some cases (e.g., ^{226}Ra) $\epsilon_p=\epsilon_f$. We consider the consequences of $\epsilon_p=\epsilon_f$ in the rotational limit. This limit is defined by the group chain

$$\begin{array}{ccccccccccccc} \mathrm{U}_{spdf}(16) & \supset & \mathrm{U}_{sd}(6) & \otimes & \mathrm{U}_{pf}(10) & \supset & \mathrm{SU}_{sd}(3) & \otimes & \mathrm{SU}_{pf}(3) & \supset & \mathrm{SU}_{spdf}(3) & \supset & \mathrm{O}_{spdf}(3), \\ N_B & & N_+ & & N_- & & (\lambda_+\mu_+) & & (\lambda_-\mu_-) & & (\lambda\mu) & & J \end{array} \tag{7}$$

where the quantum numbers associated with each algebra are shown. This subalgebra conserves separately the number of sd (N_+) and pf (N_-) bosons.

A simple dynamical symmetry Hamiltonian for this rotational limit is

$$H=\epsilon_-\hat{N}_- -\kappa\hat{Q}^2_{spdf}. \tag{8}$$

Here $\epsilon_-=\epsilon_p=\epsilon_f$, $\hat{N}_-=\hat{n}_p+\hat{n}_f$, and $\hat{Q}_{spdf}$ is the quadrupole operator of $\mathrm{SU}_{spdf}(3)$ [see Eq. (2)]. This Hamiltonian is similar to that used in the fits presented in Sec. II [Eq. (1)] with a few notable exceptions. In our study, the positive parity states have a transitional structure breaking the $\mathrm{SU}_{sd}(3)$ limit, so that the additional interaction $\epsilon_d\hat{n}_d$ is required. For the negative parity states, the $\mathrm{SU}_{pf}(3)$ symmetry is restored only in certain nuclei where $\epsilon_p=\epsilon_f$. In this case the Casimir operator of $\mathrm{U}_{pf}(10)$ $(\epsilon_p=\epsilon_f)$ can be used [see Eq. (7)] instead of breaking this symmetry to $\mathrm{U}_f(7)\otimes\mathrm{U}_p(3)$ $(\epsilon_p\neq\epsilon_f)$, and one can still have rotational symmetry for the negative parity states. As we mentioned earlier, there are some sign ambiguities in the definition of $\hat{Q}_{sd}$ and $\hat{Q}_{pf}$, the generators of $\mathrm{SU}_{sd}(3)$ and $\mathrm{SU}_{pf}(3)$. In $\hat{Q}_{sd}$ we can choose $\chi^{(2)}_{sd}=\pm\sqrt{7}/2$. In the decomposition (7), the choice $\chi^{(2)}_{sd}=-\sqrt{7}/2$ corresponds to $(\lambda_+\mu_+)$ and prolate quadrupole deformation, while $\chi^{(2)}_{sd}=+\sqrt{7}/2$ corresponds to the conjugate representation $(\mu_+\lambda_+)$ and oblate quadrupole deformation. In the IBM-1, this difference in representations is indistinguishable except in the sign of the quadrupole moments.

A similar behavior holds for $\chi^{(2)}_{pf}=\pm 1$ in $\hat{Q}_{pf}$. When $\chi^{(2)}_{pf}=-1$ we have $(\lambda_-\mu_-)$, while $\chi^{(2)}_{pf}=+1$ corresponds to $(\mu_-\lambda_-)$. In this case we do not have a simple geometric interpretation of the shapes.

When we consider the spectra of $\mathrm{SU}_{spdf}(3)$, we must obtain the allowed quantum numbers by coupling the representations of $\mathrm{SU}_{sd}(3)$ to $\mathrm{SU}_{pf}(3)$. It is at this point that the ordering $(\lambda\mu)$ or $(\mu\lambda)$ makes a difference. When we choose $\mathrm{sgn}(\chi^{(2)}_{sd},\chi^{(2)}_{pf})=(-,-)$ or $(+,+)$, we obtain a particular set of $(\lambda\mu)$. If we choose instead $(+,-)$ or $(-,+)$ we obtain a different set of quantum numbers. Consequently, the dipole-octupole excitation built on prolate or oblate ground states will have distinct features. The allowed ranges of these quantum numbers have been recently studied by Ibrahim [44].

The spectrum of Eq. (7) is given by

$$E=\epsilon_-N_- -\frac{\kappa}{2}[\lambda^2+\mu^2+\lambda\mu+3(\lambda+\mu)]+\frac{3}{8}\kappa J(J+1). \tag{9}$$

The allowed range of $(\lambda\mu)$ is obtained from the coupling $(\lambda_+\mu_+)\otimes(\lambda_-\mu_-)$ for $\mathrm{sgn}(\chi^{(2)}_{sd},\chi^{(2)}_{pf})=(-,-)$, or $(+,+)$ or from the coupling $(\mu_+\lambda_+)\otimes(\lambda_-\mu_-)$ [or $(\lambda_+\mu_+)\otimes(\mu_-\lambda_-)$] for $\mathrm{sgn}(\chi^{(2)}_{sd},\chi^{(2)}_{pf})=(-,+)$ [or $(+,-)$]. The situation $\mathrm{sgn}(\chi^{(2)}_{sd},\chi^{(2)}_{pf})=(-,-)$ corresponds to our numerical study and we show in Fig. 10 a typical spectrum corresponding to this symmetry choice in Eq. (9) $(\kappa>0)$.

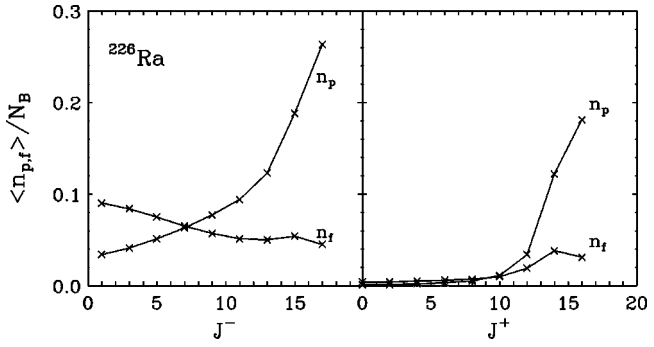

FIG. 9. Negative parity boson content in yrast states as a function of spin in ^{226}Ra for the calculations with $3pf$ bosons using the Hamiltonian in Eqs. (1) and (5).

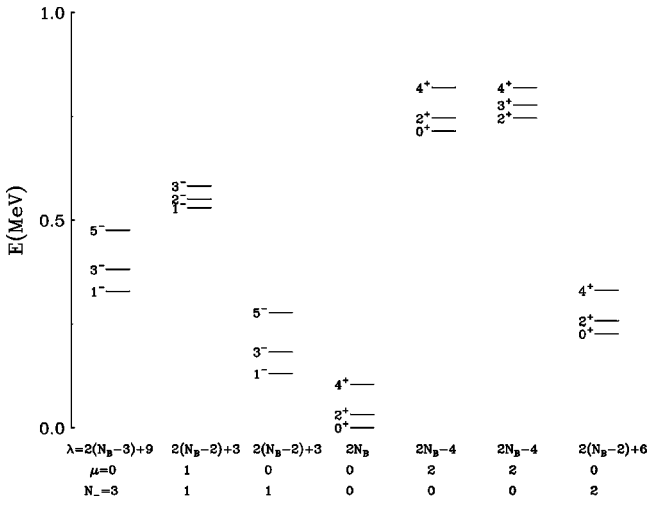

FIG. 10. Spectra of the $SU_{spdf}(3)$ Hamiltonian [Eq. (9)] for $N_B=9$ ($\epsilon_-=0.4$ MeV, $\kappa=0.014$ MeV). The quantum numbers N_-, λ, and μ are given for each band.

Here the quantum numbers $(\lambda\mu)$, N_-, and J^π are all indicated. One immediate observation is that the ground state is not dipole-octupole deformed since $N_- = 0$. Rather, this deformation ($N_-=2$) sets in at higher excitation energy given by $\Delta E=2\epsilon_- - \kappa(4N+5)$.

In general, the Hamiltonian (8) allows ground state quadrupole deformation ($N_+>0$) or ground state octupole deformation ($N_->0$) but not both. The reason is as follows: For $\epsilon_->0$, the lowest energy band will have $(\lambda,\mu)=(2N_B,0)$ and describes states with $N_-=0$ and $N_+=N_B$. The states with maximum octupole deformation, $(\lambda\mu)=(3N_B,0)$, where $N_-=N_B$ are higher in the spectra due to the energy offset $\epsilon_- N_-$. When $\epsilon_-\to 0$, these maximally octupole deformed states becomes yrast and have $N_-=N_B$ (or N_B-1 if N_B is odd). Hence the ground state has either maximum N_+ or $N_-(=N_B-N_+)$ but not both.

Another feature of this rotational limit is that molecular bands $(0^+,1^-,2^+,3^-,\ldots)$ can only occur by accident. For example, interleaving dipole-octupole deformed $K^\pi=0^+$ $(N_-=2)$ and $K^\pi=0^-$ $(N_-=3)$ bands will occur if $\epsilon_-=\kappa(2N_B+4)$. In Fig. 10 this would correspond to adjusting the energy of the leftmost and rightmost bands so that they interleave. This correction changes $\epsilon_-=0.4$ MeV (used in the figure) to $\epsilon_-=0.31$ MeV. But, as we mentioned earlier, this does not change the octupole character of the bands.

IV. CONCLUSION

We obtained a consistent picture over the entire nuclear region of the light actinides using a simple Hamiltonian in the $spdf$ space of the IBM. The structure of the low-lying states are found to have at most $1pf$ boson, which is equivalent to the lack of ground state dipole-octupole deformation. However, the behavior of $E1$ matrix elements in ^{226}Ra for $J\geqslant 12\hbar$ shows that the octupole correlations increase with spin and at a medium spin ($J\sim 12\hbar$) there is an onset of dipole-octupole deformation in agreement with a phenomenological analysis [45]. It appears that in the ground state these nuclei are soft against dipole-octupole deformation but rotation stabilizes the dipole-octupole deformation.

ACKNOWLEDGMENTS

Valuable discussions with Rick Casten are gratefully acknowledged. This work was supported by the U.S. DOE Grant Nos. DE-FG02-91ER-40609 and DE-FG02-88ER-40417.

[1] For a review, see P.A. Butler and W. Nazarewicz, Rev. Mod. Phys. **68**, 349 (1996).
[2] W. Nazarewicz, P. Olanders, I. Ragnarsson, J. Dudek, G.A. Leander, P. Möller, and E. Ruchowska, Nucl. Phys. **A429**, 269 (1984).
[3] F. Iachello and A. Arima, *The Interacting Boson Model* (Cambridge University Press, Cambridge, 1987).
[4] F. Iachello and A. Arima, Phys. Lett. **53B**, 309 (1974).
[5] A. Arima and F. Iachello, Ann. Phys. (N.Y.) **99**, 253 (1978); **111**, 201 (1978).
[6] A.F. Barfield, B.R. Barrett, J.L. Wood, and O. Scholten, Ann. Phys. (N.Y.) **182**, 344 (1988).
[7] P.D. Cottle and N.V. Zamfir, Phys. Rev. C **54**, 176 (1996).
[8] P.D. Cottle and N.V. Zamfir, Phys. Rev. C **58**, 1500 (1998).
[9] C.S. Han, D.S. Chuu, S.T. Hsieh, and H.C. Chiang, Phys. Lett. **163B**, 295 (1985).
[10] J. Engel and F. Iachello, Phys. Rev. Lett. **54**, 1126 (1985); Nucl. Phys. **A472**, 61 (1987).
[11] Dimitri Kusnezov, Ph.D thesis, Princeton University, 1988
[12] Dimitri Kusnezov and F. Iachello, Phys. Lett. B **209**, 420 (1988).
[13] D.F. Kusnezov, E.A. Henry, and R.A. Meyer, Phys. Lett. B **228**, 11 (1989).
[14] M. Sugita, T. Otsuka, and P. von Brentano, Phys. Lett. B **389**, 642 (1996).
[15] T. Otsuka and M. Sugita, Phys. Lett. B **209**, 140 (1988).
[16] I.N. Mikhailov, E.G. Nadjakov, M. Aiche, Ch. Briancon, N. Schulz, and V. Vanin, J. Phys. G **15**, L19 (1989).
[17] V.S. Lac and I. Morrison, Nucl. Phys. **A581**, 73 (1995).
[18] A.F. Diallo *et al.*, Ann. Phys. (N.Y.) **279**, 81 (2000).
[19] Dimitri Kusnezov, J. Phys. A **22**, 4271 (1989); **23**, 5673 (1990).
[20] E.G. Nadjakov and I.N. Mikhailov, J. Phys. G **13**, 1221 (1987).
[21] T. Otsuka, Phys. Lett. B **182**, 256 (1986).
[22] N.V. Zamfir, O. Scholten, and P. von Brentano, Z. Phys. A **337**, 293 (1990).
[23] D.D. Warner and R.F. Casten, Phys. Rev. C **28**, 1798 (1983).
[24] P.O. Lipas, P. Toivonen, and D.D. Warner, Phys. Lett. **155B**, 295 (1985).
[25] Dimitri Kusnezov, computer code OCTUPOLE (unpublished).
[26] W.-T. Chou, N.V. Zamfir, and R.F. Casten, Phys. Rev. C **56**, 829 (1997).

[27] W. Kurcewicz *et al.*, Nucl. Phys. **A270**, 175 (1976).
[28] M. Wieland *et al.*, Phys. Rev. C **46**, 2628 (1992).
[29] E. Ruchowska *et al.*, Nucl. Phys. **A383**, 1 (1982).
[30] D. Ward *et al.*, Nucl. Phys. **A406**, 591 (1983).
[31] W. Bonin *et al.*, Z. Phys. A **322**, 59 (1985).
[32] Y. Gono *et al.*, Nucl. Phys. **A459**, 427 (1986).
[33] P. Schüller *et al.*, Phys. Lett. B **174**, 241 (1986).
[34] R.J. Poynter *et al.*, Phys. Lett. B **232**, 447 (1989).
[35] N. Schulz *et al.*, Phys. Rev. Lett. **63**, 2645 (1989).
[36] B. Ackermann *et al.*, Nucl. Phys. **A559**, 61 (1993).
[37] H.J. Wollersheim *et al.*, Nucl. Phys. **A556**, 261 (1993).
[38] J.F. Smith *et al.*, Phys. Rev. Lett. **75**, 1050 (1995).
[39] J.F.C. Cocks *et al.*, Phys. Rev. Lett. **78**, 2920 (1997); Nucl. Phys. **A645**, 61 (1999).
[40] T. Weber *et al.*, Eur. Phys. J. A **1**, 39 (1998).
[41] T. Weber *et al.*, Eur. Phys. J. A **3**, 25 (1998).
[42] K. Guldal *et al.*, Nucl. Phys. **A636**, 28 (1998).
[43] M.R. Schmorak, Nucl. Data Sheets **63**, 139 (1991); Y. A. Akovali, *ibid.* **69**, 155 (1993); **76**, 457 (1995); **77**, 271 (1996); **77**, 433 (1996); Agda Artna-Cohen, *ibid.* **80**, 157 (1997); **80**, 227 (1997); **80**, 723 (1997).
[44] M. Ibrahim, Ph.D. thesis, Yale University, 2000.
[45] N.V. Zamfir, P. von Brentano, and R.F. Casten, Phys. Rev. C **49**, R605 (1994).